PHILOSOPHICAL TRANSACTIONS OF THE ROYAL SOCIETY A MATHEMATICAL, PHYSICAL & ENGINEERING SCIENCES

Development of the Temperature and Salinity Structure of the Upper Ocean over Two Months in an Area 150 $\times $ 150 km [and Discussion]

G. J. Prangsma, T. H. Guymer, P. Kruseman, R. T. Pollard, R. A. Weller and G. Siedler

Phil. Trans. R. Soc. Lond. A 1983 **308**, 311-325
doi: 10.1098/rsta.1983.0006

Phil. Trans. R. Soc. Lond. A. **308**, 311–325 (1983)
Printed in Great Britain

Development of the temperature and salinity structure of the upper ocean over two months in an area 150×150 km

By G. J. Prangsma†, T. H. Guymer‡, P. Kruseman†, R. T. Pollard‡ and R. A. Weller§

† *Koninklijk Nederlands Meteorologisch Instituut, De Bilt, Netherlands*
‡ *Institute of Oceanographic Sciences, Wormley, Godalming, Surrey GU8 5UB, U.K.*
§ *Woods Hole Oceanographic Institution, Woods Hole, Massachusetts* 02543, *U.S.A.*

During the two months of the JASIN experiment a regular conductivity–temperature–depth station pattern was worked by Hr. Neth. Ms. *Tydeman*, giving a total of eight surveys of temperature and salinity structure in an area 100 km × 150 km. The data are averaged to obtain hourly and spatial mean profiles. It is shown that this averaging conserves heat and salt content. The spatial mean profiles are compared with heat budget computations, and it is found that, on average, surface heat fluxes dominate the time history of the oceanic heat content on the scale of the whole survey area. On smaller scales advection due to mesoscale structures dominates, masking any differences in heating in different water masses. Comparison with results from a one-dimensional mixed-layer model indicates that this type of model satisfactorily simulates the development of the temperature profile as a spatial average for the survey area.

1. Introduction

In studies of the effects of air–sea interaction on the upper ocean layers there are at least two major difficulties to be overcome before changes in the structure of the water column resulting from surface fluxes can be resolved.

First, there is the enormous variability both in space and in time in the upper ocean, as a consequence of

the (horizontal) mesoscale features (eddies, fronts),

the (vertical) internal wave activity in pycnoclines on shorter time scales (of order one hour and less),

processes (horizontal and vertical) on longer time scales (tides, inertial motion).

Second, there is a clear mismatch in temporal and spatial scales of the two media involved in air–sea interaction. The spatial scales of the features relevant to our problem are of order 10–100 km in the upper ocean (width of fronts, eddy sizes) and of order 100–1000 km (and more) in the atmosphere, and the time scales on which significant changes occur range from hours in the atmosphere to days and weeks in the ocean. Typical horizontal velocity scales are 10 cm s^{-1} in the upper ocean and 10 m s^{-1} in the atmosphere.

These scale differences provide a strong motivation for studying the influence of air–sea interaction on the upper ocean structure in a horizontally averaged sense only. This motivation can be explained as follows: the larger-scale atmospheric features propagate at such a speed that the surface fluxes will be determined by the oceanic parameters 'smoothed' over the atmospheric scales, i.e. the gross balances of the quantities will be determined by averaged oceanic surface parameters rather than local values, the upper-ocean mesoscale variability thus being averaged over the horizontal scales of the atmospheric structure. In other words,

it seems natural to use one-dimensional air–sea interaction models for the ocean, where such a model should be representative for a piece of ocean of the size of atmospheric features. One is then left with the problem of averaging ocean observations, which include the oceanic mesoscale structure to the extent of being 'representative' for a fairly large area, encompassing

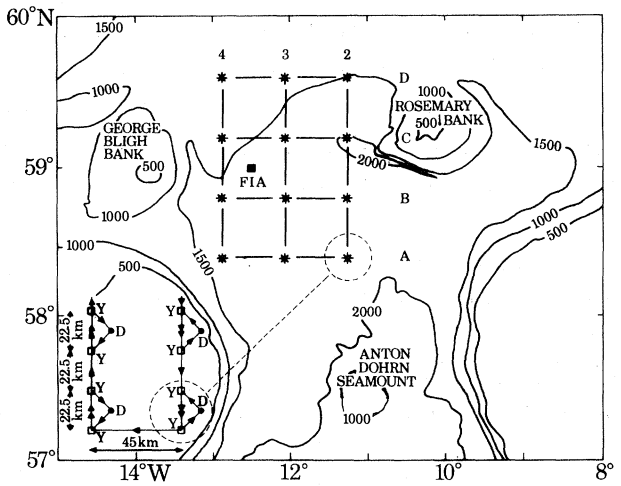

FIGURE 1. North Rockall Trough with grid pattern of stations worked by Hr. Neth. Ms. *Tydeman*. Inset: each gridpoint consisted of a deep station (D) at the nominal grid position and two yoyo stations (Y) worked twice with a 6–6¼ hour interval between workings. The position of the Fixed Intensive Array (FIA) is indicated.

TABLE 1. INVENTORY OF ONE-HOUR CTD YOYO STATION DATA FROM *TYDEMAN*

survey	dates (1978)	number of stations worked	number of useful stations
1	17–22 Jul.	52	27
2	22–28 Jul.	44	24
3	28 Jul. – 4 Aug.	44	44
4	4–10 Aug.	45	45
5	21–26 Aug.	51	51
6	26 Aug. – 2 Sep.	38	37
7	2–8 Sep.	36	36
8	8–14 Sep.	46	46

usually some (parts of) mid-ocean eddies, fronts and other phenomena. The averaging procedure should conserve heat and salt. The procedure used in this study will be outlined in §3 after a description of the available data in §2. The profiles are described in §4 and contributions to the heat budget are discussed in detail in §5. In §6 results from model computations will be compared with the averaged profiles. Among the questions to be considered are:

How does heat storage change as a function of depth during the JASIN period?

What spatial averaging is required to reduce horizontal advection of heat to a small fraction of surface heat flux?

Can heating of the thermocline below the directly wind-mixed layer be detected and can we distinguish between mechanisms that might cause it (vertical motion at fronts, internal mixing, Ekman pumping)?

PHILOSOPHICAL TRANSACTIONS OF THE ROYAL SOCIETY A MATHEMATICAL, PHYSICAL & ENGINEERING SCIENCES

2. Description of *Tydeman* data set

During the JASIN experiment a regular conductivity–temperature–depth (CTD) station grid was worked by Hr. Neth. Ms. *Tydeman*. The basic pattern (figure 1, inset) consisted of two yoyo CTD stations, 22.5 km apart, and one deep CTD station. Each yoyo station, consisting of continuous CTD profiling in the upper (200–250 m) ocean layer for about one hour, was occupied twice with an interval of 6–6¼ hours between occupations to allow reduction of tidal variations by averaging. The deep station, down to within 50 m of the bottom, included also a near-surface water-bottle comparison in all those cases where a well defined surface mixed layer was observed. The basic pattern was worked around the grid points in the hydrographic mapping area (figure 1) on tracks oriented either north–south or east–west, a total of eight survey patterns being thus obtained, each of which took about five days to complete. The deep CTD stations were part of the hydrographic mapping exercise discussed by Ellett *et al.* (this symposium). The water-bottle comparisons were used along with intercomparison stations with R.V. *Meteor* and R.R.S. *Challenger* and independent sensor calibrations to get a full check on our CTD system, including the data logger. Agreement to within 0.01‰ or less in salinity and of 0.01 K or less in temperature was found, except in parts of the water column influenced by fronts.

On several occasions yoyo CTD stations of long duration (typically 10–24 hours) were worked to provide a data set for case studies on the daily heating–cooling cycle. These data will be discussed elsewhere. The data from the one-hour yoyo stations, after editing and calibration checks, stations with instrumental problems being disregarded, amount to a total of 310 stations distributed over eight surveys (see table 1) and have been used in the analysis described in the remainder of this paper.

3. Averaging procedures for CTD profiles

As outlined, it is convenient to distinguish between two kinds of variability when comparing real ocean measurements with model-derived data: short-term variability due to high frequency internal wave activity (of order one hour or less) and spatial variability on the mid-ocean eddy scale (of order 10–100 km) together with longer-period oscillations (tides, inertial).

Kruseman & Prangsma (1977), for example, found tidal-period variations of over 20 dynamic mm in the dynamic thickness of a 600 dbar† layer (500–1100 dbar) in the JASIN area in 1977. The eddy-scale spatial structure in our present survey area is described by Ellett *et al.* (this symposium) and Pollard (1982*a*). The averaging procedure can thus naturally be split up into two separate stages: first, average the one-hour yoyo series to remove short-period internal waves and create a single profile for each station; second, average all the one-hour mean profiles in a single survey. The second averaging procedure reduces eddy-scale spatial variability as well as tidal–inertial period oscillations.

Averaging yoyo data and conservation of heat and salt

For our study it is essential to understand what type of averaging should be applied and

† bar = 10^5 Pa.

what are its limitations. Consider the contribution to the heat content from a single profile i (ΔH_i) from the (infinitesimally small) layer bounded by densities $\rho_1(S, T, p)$ and $\rho_2(S, T, p)$

$$\begin{aligned}\Delta H_i(\rho_1, \rho_2) &= \int_{\rho_1}^{\rho_2} \rho' c_p T_i(\rho')\, \mathrm{d}\rho' \\ &\approx \rho c_p T_i(\rho)\, \Delta\rho, \end{aligned} \tag{1}$$

where T is temperature and c_p specific heat at constant pressure. Averaging over density (σ_t) surfaces gives

$$\begin{aligned}\overline{\Delta H_i(\rho_1, \rho_2)} &= \overline{\rho c_p T_i(\rho)\, \Delta\rho} = c_p\, \Delta\rho\ \overline{\rho T_i(\rho)} \\ &= c_p\, \Delta\rho\{\bar{\rho}\,\overline{T(\rho)} + \overline{(\rho - \bar{\rho})\,[T_i(\rho) - \overline{T(\rho)}]}\} \\ &= \overline{\Delta H(\rho_1, \rho_2)} + c_p\, \Delta\rho\,\overline{(\rho - \bar{\rho})\,[T_i(\rho) - \overline{T(\rho)}]}. \end{aligned} \tag{2}$$

The last term on the right-hand side of equation (2) is always negative, indicating that averaging over σ_t surfaces is not conservative for heat content. Averaging on density ($\rho(S, T, p)$) surfaces, however, yields

$$\begin{aligned}\overline{\Delta H_i(\rho_1, \rho_2)} &= \overline{\rho c_p T_i(\rho)\, \Delta\rho} \\ &= \rho c_p\, \Delta\rho\, \overline{T(\rho)} = \Delta\overline{H(\rho_1, \rho_2)}, \end{aligned} \tag{3}$$

which does not contain any cross-correlation terms and is in consequence conservative for heat content. The same argument can be applied to salt conservation.

Accordingly we have averaged on $\rho(S, T, p)$ surfaces, both for the one-hour yoyo series and for the spatial averaging. For the spatial averaging of mean station profiles one more complication arises since the presence of eddies causes differences in the surface density. In other words, for densities less than the maximum surface density in the area, there are stations that do not contribute to the spatially averaged profile. To solve this problem one first applies the foregoing averaging procedure between the minimum (ρ_m) and maximum densities present in *all* profiles. Then the surface parts of the profiles are shrunk or stretched in such a way that each data point is transferred from the observed pressure p_obs to a pressure p_prof by

$$p_\mathrm{prof} = p_\mathrm{obs} p_{\rho\mathrm{m}} / \bar{p}_{\rho\mathrm{m}}$$

where $p_{\rho\mathrm{m}}$ is the depth of the minimum density in the profile being stretched or shrunk and $\bar{p}_{\rho\mathrm{m}}$ is the (spatial) mean depth of the minimum density surface. The resultant profiles were then averaged on the adjusted pressure.

This approach can be shown to be conservative for salt and heat content under the assumption that the amount of water between any two isopycnal layers is constant in the mean over a large enough area. Further details of the averaging procedure may be found in Kruseman & Prangsma (1982).

4. Development of T, S structure

The eight sets of *Tydeman* survey-averaged profiles are shown in figure 2, and derived Brunt–Väisälä frequency profiles in figure 3. The standard deviations shown are on density surfaces and are those appropriate to the one-hour-averaged yoyo profiles. They are generally less than 5 dbar, 0.3 K and 0.05‰ in pressure, temperature and salinity respectively. The standard deviations of the mean profiles would be reduced by the square root of the number of useful stations in the survey (table 1) to less than 1 dbar, 0.06 K and 0.01‰.

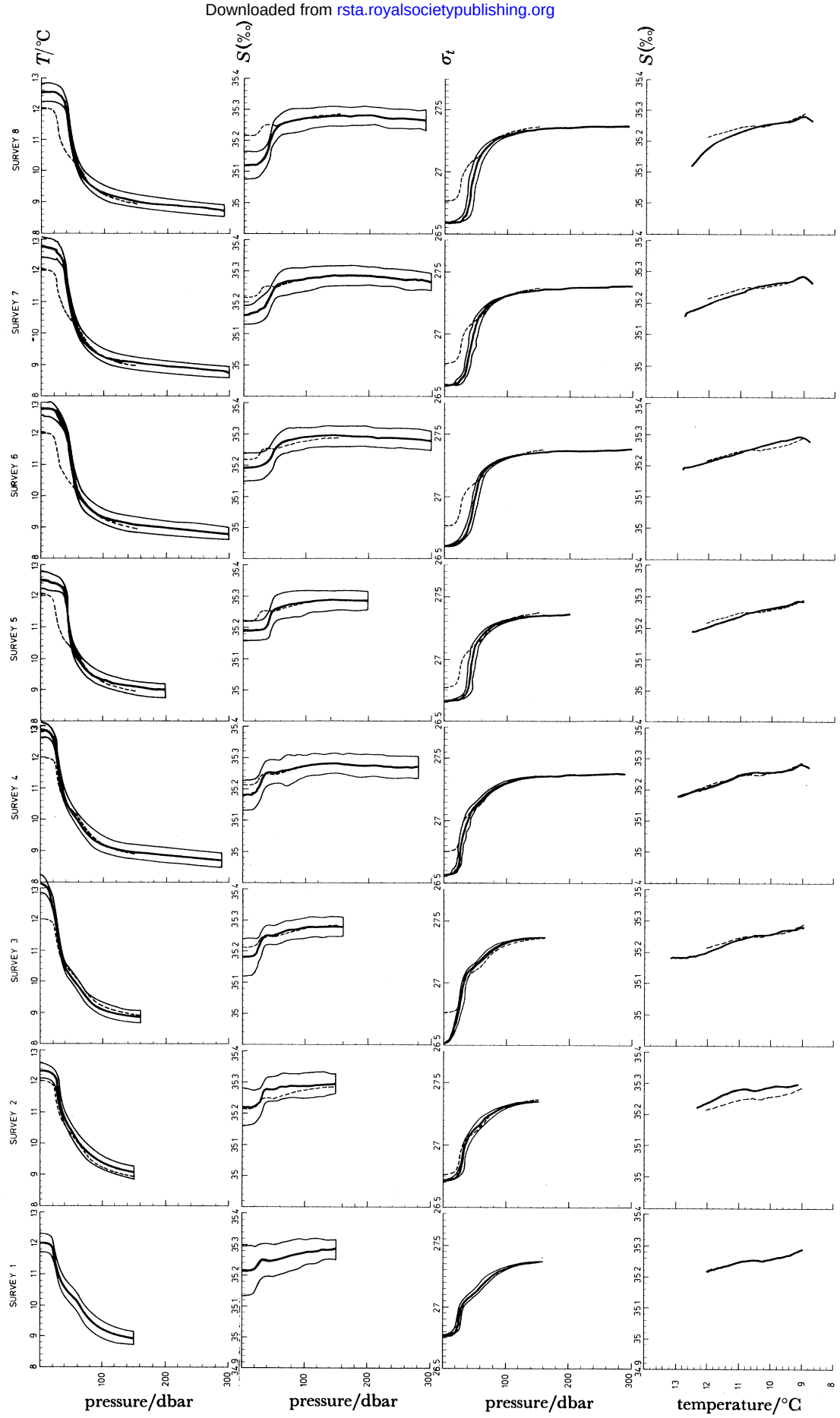

FIGURE 2. Area mean profiles for surveys 1–8. From top to bottom: temperature, salinity, σ_t and T,S diagram. For comparison the corresponding profile of survey 1 is indicated (– – –). Standard deviations of the one-hour averaged profiles are shown by thin lines.

From table 1 it is clear that in surveys 1 and 2 – owing to instrumental problems – an appreciable number of stations are missing, namely the easternmost line of stations for survey 1 and the northern two lines for survey 2. Since the eddy structure as discussed by Ellett *et al.* (this symposium) has almost no influence on the easternmost line of stations, the result for survey 1 can still be considered to be representative for the temperature and salinity distribution at that time. This conclusion is confirmed by comparing the result for survey 3 with an averaged

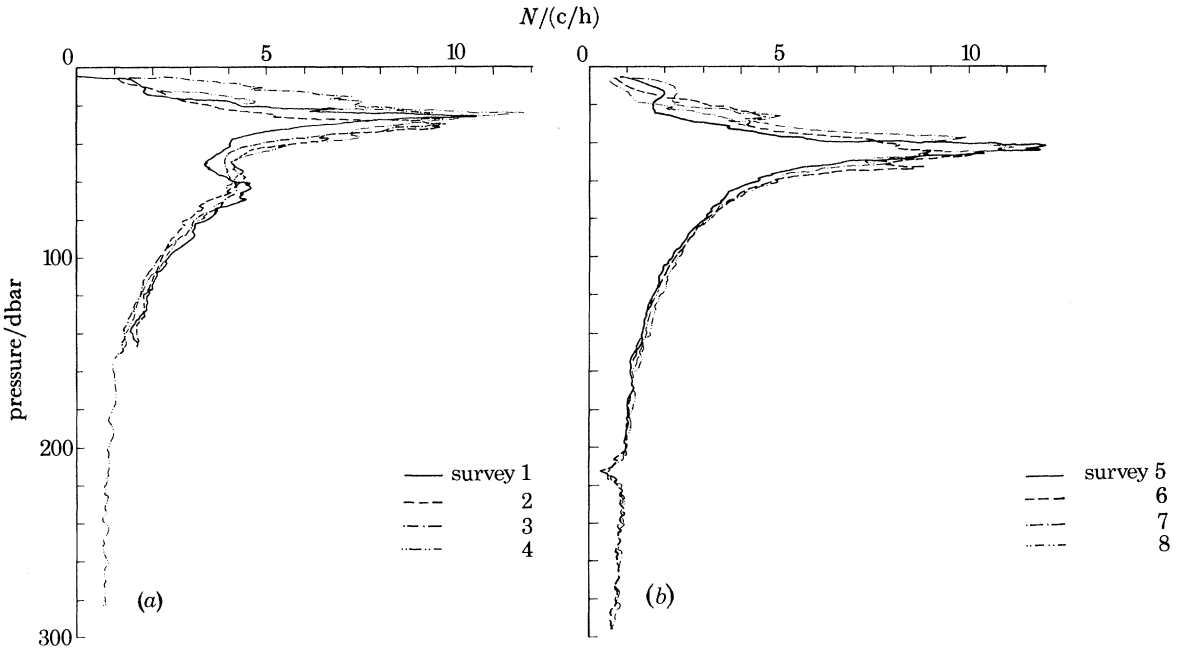

FIGURE 3. Brunt–Väisälä frequency, N, for mean profiles in (*a*) phase 1 and (*b*) phase 2.

profile for the survey 3 period leaving out the stations along the eastern line, and also by the fact that the overall T, S structure of survey 1 is in line with the T, S structure found in surveys 3–8. The mean profiles for survey 2, however, are biased to the higher temperatures and salinities present in the southern part of the hydrographic mapping area (figure 2, survey 2, T, S diagram).

Chronological description of T, S development

Early in the JASIN experiment T, S profiles are characterized by a mixed layer 10–20 m deep. In the seasonal thermocline between 40 and 80 m a clearly distinguishable tongue of relatively warm and saline water from the south is advected northward on the western edge of the underlying eddy structure. (Pollard *et al.* this symposium, figure 5). This saline water, observed at the southwestern gridpoints, causes the salinity maximum in the top of the seasonal thermocline and is found in the temperature profiles as a kink around 60–70 m. The combination of these features results in a secondary maximum in the Brunt–Väisälä frequency at 50–70 m at the individual stations (mainly at C 4, C 3, B 4, B 3 and A 3) as well as in the averaged profile (figure 3). The kink in the T, S diagram around 10.5 °C (figure 2) is also due to the advected southern warm water.

In survey 2 (22–28 July) the profiles are biased towards the southern warm and saline wates as discussed. The salinity maximum is still present as is the relative maximum in the Brunt–Väisälä frequency around 60 m.

During the first days of survey 3 (28 July to 4 August) rapid heating occurred in the top few metres, with no clearly definable mixed layer. Wind mixing during the last two days (3 and 4 August) resulted in mixed-layer depths of 15–20 m. In the mixed layer the advection of water of lower salinity from the north or northwest becomes apparent as a 0.02–0.03‰ salinity deficit in the mean. The warm, saline tongue of water in the western part of the area is less pronounced in the individual profiles, but remains discernible in the Brunt–Väisälä (figure 3) and T, S (figure 2) profiles. Survey 4 (4–10 August) experienced some stronger winds, causing the mixed layer to deepen to between 15 and 25 m.

Throughout phase 1 the general structure of the Brunt–Väisälä frequency profiles (figure 3*a*) is similar, with maximum values of 10–12 cycles per hour (c/h) between 20 and 30 m and a secondary maximum of about 4 c/h around 60 m, the latter becoming gradually less pronounced.

During 10–20 August strong wind-mixing occurred (Pollard *et al.*, this symposium) leading to mixed-layer depths of 30–40 m (or slightly deeper in some locations) as found in survey 5 (21–26 August) at the start of phase 2. Heating continued, resulting in some restratification later in the survey with mixed-layer depths around 20 m. The tongue of warm, saline water can no longer be identified and the kink in the temperature profile, the salinity maximum in the top of the seasonal thermocline, the secondary maximum in the Brunt–Väisälä frequency and the T, S structure around 10.5 °C have disappeared.

Apart from continued heating (0.3 K in the mean sea-surface temperature) survey 6 (26 August to 2 September) compares with survey 5. Survey 7 (2–8 September) is characterized by a strong mixing event on 4 September resulting in mixed-layer depths of 30–40 m and slightly deeper in one or two yoyo profiles. Afterwards, restratification again occurred in the top 10–20 m. The growing salt deficit in the top layers becomes more marked, especially in the T, S diagram, indicating the advection of water of lower salinity in the mixed layer. This advection continues strongly during survey 8 (8–14 September), when strong winds during the last days of the JASIN field phase cause cooling (0.2 K in the mean sea surface temperature) and mixing down to 40 m and more.

The general structure of the Brunt–Väisälä frequency profiles in phase 2 (figure 3*b*), with a maximum value of 10–12 c/h around 50 m is similar to those in phase 1 (figure 3*a*), except for the disappearance of the secondary maximum around 60 m. The similarity of the Brunt–Väisälä profiles during the whole of JASIN, apart from a shift in depth in mid-August, lends some support to similarity profile models for the mixed layer and the underlying seasonal thermocline (see for example Kitaigorodskii & Miropolskii 1970).

5. Heat budget

Contributions to the vertically integrated heat budget can arise from surface fluxes, horizontal advection and heat storage. The vertical distribution of heat may contain contributions from radiative input decaying with depth, wind-driven mixing in the surface layer, mixed-layer deepening and Ekman convergence. Diffusion in the thermocline may also be affected by internal wave breaking and vertical transport at fronts. Let us consider to what extent we can separate and quantify these contributions.

Surface fluxes

In §1 it was argued that the relatively high propagation speed of the atmospheric forcing fields smooths considerably the variability in air–sea fluxes. Although clear differences in

PHILOSOPHICAL TRANSACTIONS OF THE ROYAL SOCIETY A MATHEMATICAL, PHYSICAL & ENGINEERING SCIENCES

TABLE 2. COMPARISON OF SURFACE HEAT FLUXES IN W/m^2

	Gardline Endurer	*Meteor*	*Hecla/John Murray*	triangle average	*Tydeman*
overall mean					
sensible heat	6 ± 4	4 ± 6	2 ± 8	4 ± 6	3 ± 6
latent heat	30 ± 20	22 ± 19	19 ± 19	24 ± 18	24 ± 21
net radiation	86 ± 40	97 ± 47	89 ± 56	91 ± 44	88 ± 51
net flux into ocean	49 ± 49	73 ± 53	67 ± 65	63 ± 52	60 ± 60
excess above Tydeman					
sensible heat	2 ± 4	0 ± 1	-2 ± 4	0 ± 2	
latent heat	8 ± 13	-3 ± 6	-5 ± 14	-1 ± 8	
net radiation	-2 ± 37	9 ± 22	2 ± 30	3 ± 23	
net flux into ocean	-10 ± 42	14 ± 24	8 ± 31	4 ± 26	

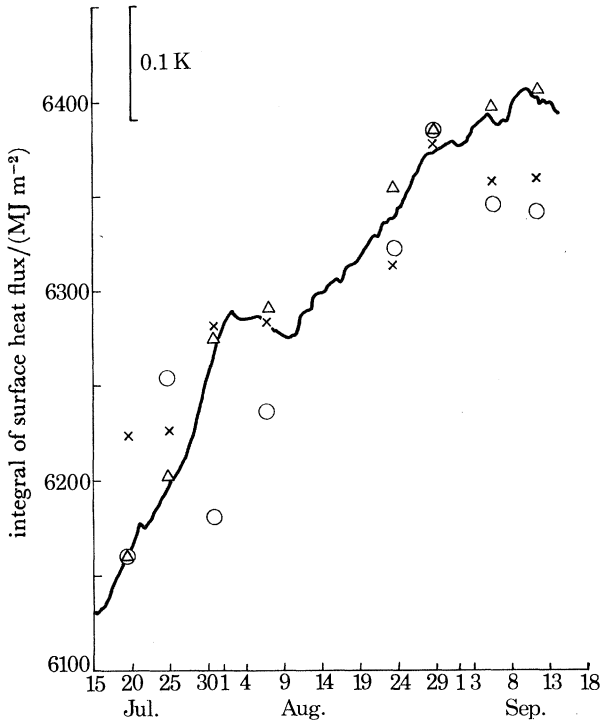

FIGURE 4. Development of the time integral of surface heat fluxes (solid line), adjusted to fit the observed heat content of the upper 150 m of the ocean in survey 1. Also shown are heat content at 150 m (circles), modelled heat content (triangles), and heat content corrected to reduce eddy effects (see text) and adjusted to match the surface heat flux curve in survey 4 (crosses).

surface fluxes have been found between the three corners of the meteorological triangle (Guymer *et al.* this symposium), the question remains open as to the extent that surface fluxes computed from observational data (solar radiation, standard World Meterological Organization (WMO) hourly synoptic observations) from a single roving ship (*Tydeman*) are representative for the area in the mean.

We therefore compared the surface heat fluxes in two ways (table 2):

daily mean fluxes of net radiation, sensible and latent heat and the net heat input into the ocean for each of the corner ships, for the triangular average of the three corner ships

and for the roving ship have been averaged for all days (totalling 24) where all four ships had complete data;

the daily differences between the roving ship and each of the corner ships were averaged. The differences between the results for the roving ship and the triangular mean results are well within the standard deviations, as are the differences between the former and results for each of the corner ships. We conclude that the surface fluxes derived from data from the roving ship are representative in the mean.

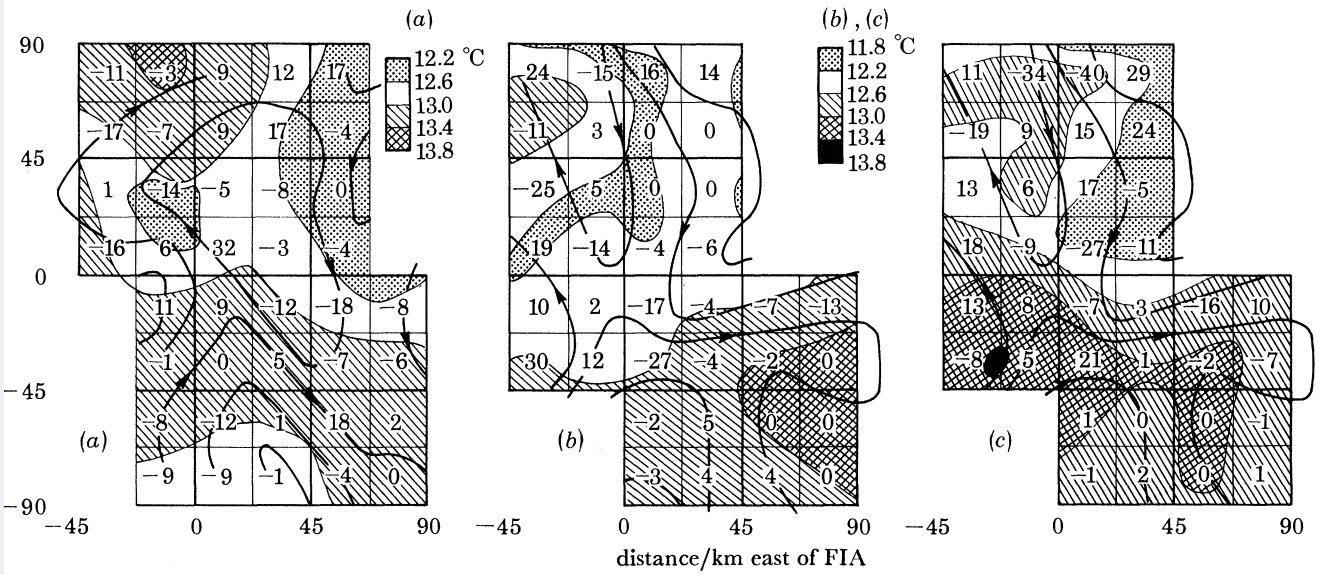

FIGURE 5. Superimposed temperature (Guymer *et al.* this symposium) and dynamic height (Pollard 1982*a*) fields are used to estimate the geostrophically advected heat flux across the sides of a 22.5 km × 22.5 km grid. The resulting advective heating rates are shown in each box in multiples of 10 W m^{-2}. Sea surface temperatures were estimated for (*a*) 4–10 August, (*b*) 21–26 August, (*c*) 27 August–5 September. Geostrophic velocities were estimated for (*a*) 31 July–9 August, (*b*) and (*c*) 21–29 August.

The observations made by *Tydeman* cover the period 17 July to 10 August, and 21 August to 14 September. To compute the integrated heat input for the JASIN period as a whole, we have used data from the W2 buoy in the Fixed Intensive Array (FIA) (Weller & Halpern this symposium) supplemented by wet-bulb temperature data from neârby ships to bridge the gap from 11 August to 20 August.

The time integral of the surface heat input is shown in figure 4 (solid line), offset by 6160 MJ/m^2, the heat content of the averaged profile of *Tydeman* survey 1 in the upper 150 m of the water column. During the last weeks of July there is strong heating, averaging 103 W m^{-2}. Then follows a period (2–10 August) of slight cooling, 22 W m^{-2}. From 11 to 28 August appreciable net heating again occurs (61 W m^{-2}). The last two weeks of JASIN are characterized by intermittent heating and cooling, resulting in a net heating of 14 W m^{-2}.

Geostrophic advection

To calculate advective heat fluxes directly, we need to know the current and temperature fields across the survey area. Direct current measurements on moorings (Pollard *et al.* this symposium) are too few to resolve the 50–100 km eddy flows (Pollard 1982*a*). We can however

estimate the velocity fields indirectly, assuming they are in either geostrophic or Ekman balance.

To calculate advection of heat by geostrophic flows, the surface temperature maps produced by Guymer *et al.* (this symposium) have been superimposed on the 10 dbar dynamic height contours derived by Pollard (1982*b*) (figure 5).

TABLE 3. RANGES OF HEATING RATES (W m^{-2}) AVERAGED OVER DIFFERENT AREAS AND COMPARED WITH SURFACE HEAT FLUXES FOR THE THREE PERIODS SHOWN IN FIGURE 5

	4–10 Aug.	21–26 Aug.	27 Aug.–5 Sep.
area		geostrophic advection	
(22.5 km)^2	−184 to 318	−270 to 298	−400 to 288
(45 km)^2	−98 to 117	−128 to 135	−81 to 70
(90 km)^2	−25 to 1	−41 to 4	−2 to 3
whole	−9	−2	5
		surface heat flux	
	−20	42	38

TABLE 4. AVERAGED WIND STRESSES FOR EIGHT-DAY PERIODS AND FOR THE WHOLE MONTH OF AUGUST

period	amplitude / N m^{-2}	direction / deg.
31 Jul.–7 Aug.	0.053	195
8–15 Aug.	0.064	320
16–23 Aug.	0.162	31
24–31 Aug.	0.067	106
31 Jul.–31 Aug.	0.038	39

The scales of temperature and velocity fields are similar (50–100 km) but the features are quite different, isotherms and dynamic height contours often being orthogonal. We infer that the temperature field is being stretched and stirred by the eddy field. Overall, cold water from the north is being drawn southward on the east side of the anticyclonic eddy and warm water from the south is drawn northward on the west side (see Ellett *et al.* this symposium). Additionally, blobs and tongues of water can be seen that have been strained by up to a complete circuit round the eddy.

A grid of squares 22.5 km × 22.5 km was superimposed on figure 5 and the temperature and geostrophic velocity component normal to each 22.5 km line segment were estimated. The advective heat flux into each box could then be calculated, if the horizontal temperature gradients were assumed to persist through some depth. We chose the mixed-layer depth 30 m in figure 5*a*, and 50 m in figures 5*b*, *c*. The resultant heat fluxes are shown in each box. They range from −400 to 300 W m^{-2} and in general dominate the surface heat flux (averaging 50 W m^{-2}, figure 4). As one might expect, the average contribution drops most markedly when the averaging area is extended to cover an eddy (90 km × 90 km, table 3), and residuals are less than 10 W m^{-2} when averaging covers the entire area (over 18 000 km^2).

Ekman advection

To estimate the contribution of the Ekman flux to heat advection, consider the eight-day wind stress averages from W 2 (table 4). The average stress was of order 0.1 N m^{-2}, but the

directions were very variable. Over the month of August the average stress was 0.04 N m^{-2} towards 39° east of north, the average being dominated by the mid-August storm. The Ekman flux $\tau\rho^{-1}f^{-1}$ would then be towards 129°, equivalent in amplitude to a velocity of 0.7 cm s^{-1} distributed through 40 m in the vertical.

To give an example of heat advection, a mean horizontal temperature gradient of 0.4 K across 100 km would lead to advection of 2.5 W m^{-2}, similar in magnitude to the geostrophic advection, and small compared with the surface heat flux. However, the Ekman and geostrophic heat fluxes cannot really be separately calculated. Although the scale of the wind field may be large compared with the eddy scale, it varies considerably with time. But even the largest short-duration stress (say 0.4 N m^{-2}) causes Ekman velocities (7 cm s^{-1} through 40 m) no larger than the geostrophic velocities (Pollard 1982*a*), and these velocities act on a temperature field dominated by the eddy stirring (figure 5). The likely effect of a strong wind acting for a few days is, then, to displace the mixed-layer temperature field by perhaps tens of kilometres relative to the (100 km scale) underlying eddy, thus contributing to and further confusing the stirring by the eddy.

Our overall conclusion is that advection of heat can be reduced to less than 10 W m^{-2} (say 20% of the surface heat flux) by averaging over an area larger than a typical eddy, in our case about 100 km × 100 km.

Advection of salinity

As an aside, it must be remarked that the same cannot be said of the salt budget. During JASIN, rainfall was minimal. Yet the salinity profiles (figure 2) all show anomalously fresh water in the mixed layer, and the anomaly increases between surveys 2 and 8 from 0.05‰ spread across 25 m to 0.14‰ across 40 m. The anomaly must be advective, and the only source of such fresh water is to the north or northwest of the region, but the details of the transport mechanism remain to be investigated.

Vertical advection

Measurements of vertical velocities in the FIA (Weller 1982) very near to a frontal feature, show a fairly systematic upwelling of 10–20 m per day (0.01–0.02 cm s^{-1}), at least ten times the Ekman suction predicted from the observed wind stress curl (Guymer *et al.* this symposium). This might – locally – have a strong influence on the thermocline structure near the front, but lack of information of vertical motion in other parts of the JASIN area prevents one from drawing any definite conclusions.

Heat storage

Consider now the heat content of a water column to depth z, defined by

$$H(z) = \int_0^z \rho(z')\, c_p\, T(z')\, \mathrm{d}z'. \tag{4}$$

H(150 m) has been calculated for the survey-averaged profiles (figure 2) and is shown by circles in figure 4. The goodness of fit to the time-integrated surface heat flux is much reduced by a number of outliers up to 80 MJ m^{-2}, or 0.13 K across 150 m, off the heating curve. Temperatures at 150 m range between surveys by nearly 0.2 K. Since surface heat fluxes penetrate negligibly to that depth, the variations are most likely residual eddy perturbations, a hypothesis that is supported by examination of the individual discrepancies. The second survey, for example, is too warm, as it is biased to the southern half of the survey area (§4).

To reduce the residual eddy signal further we calculated the heat content relative to the

PHILOSOPHICAL TRANSACTIONS OF THE ROYAL SOCIETY A MATHEMATICAL, PHYSICAL & ENGINEERING SCIENCES

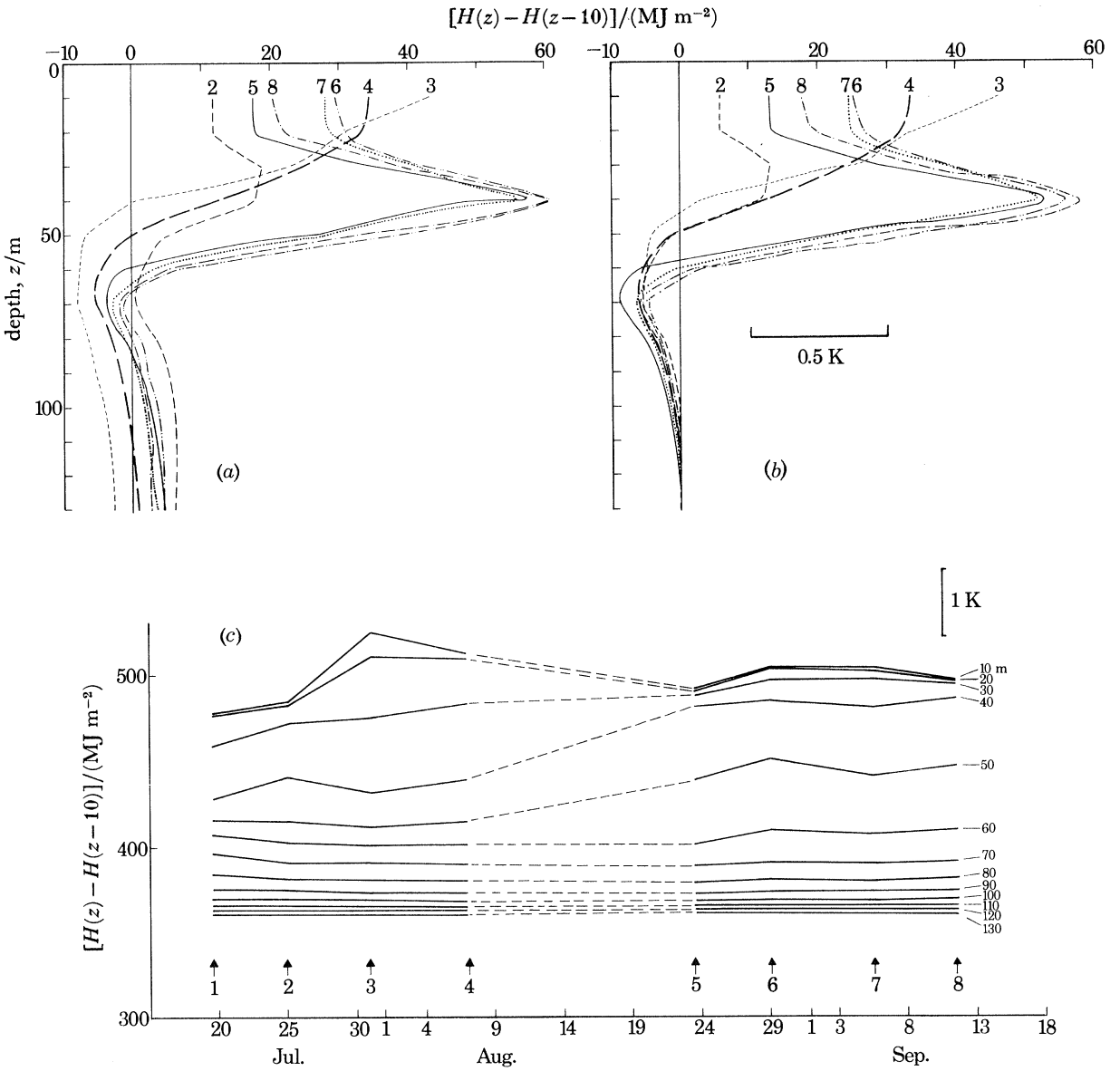

FIGURE 6. Development of heat content of layers of 10 m thickness (*a*) as observed, (*b*) after removal of the eddy signal in the 120–130 m layer, and (*c*) with time after removal of residual eddy signal in the 120–130 m layer. Arrows in (*c*) are labelled with survey number.

average temperature between 120 and 130 m, following Gill (1975), and plotted the results on figure 4 (crosses), offset so that the value for survey 4 coincided with the heating curve. With the exception of survey 1, errors are no more than 40 MJ m^{-2}, equivalent to 0.06 K across 150 m, so the goodness of fit is slightly improved. Nevertheless, the discrepancies are larger than can be attributed to advective terms, and we shall show that they are still caused by residual eddy effects.

To investigate the vertical distribution of changes in heat storage, the heat content in 10 m bands of the water column $\Delta H(z) = H(z) - H(z-10)$ has been calculated and is shown in figure 6. The main features are as follows. Between surveys 2 and 3 the large surface heat input

(110 W m^{-2}) is stored in the top 20 m. Between surveys 3 and 4, surface heating is small, but wind action redistributes heat, increasing the heat content between 20 and 50 m, diminishing that above 20 m. Strong winds between surveys 4 and 5 destroy the region of minimum N^2 between 40 and 50 m, distributing the heat by direct mixing nearly independently of depth

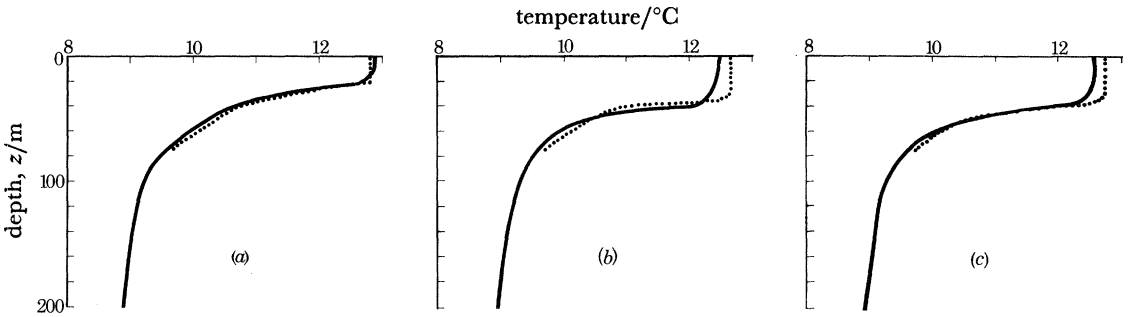

FIGURE 7. Comparison of observed (solid line) and computed (dotted line) temperature profiles for surveys (*a*) 4, (*b*) 5 and (*c*) 8.

down to 40 m. The 40–50 m heat content also increases. Between surveys 5 and 8, heat contents in layers down to 40 m increase a little, with the largest increase in the 40–50 m layer. We conclude that mixed-layer depths of over 40 m must occur over a least part of the survey area, as indeed found in several yoyo stations.

Below 60 m, all surveys show a deficit in heat content relative to survey 1, in which the relatively warm salty intrusion was most marked (figure 2). In other words, the vertical structure of the eddy signal changes between surveys, so eddy effects are not entirely removed by taking temperatures relative to 140 m (figure 6*b*). We conclude that no trend in heat content can be discerned above the noise level of variability between surveys, and that the areally averaged temperature profiles are insufficient to resolve any heating of the thermocline below the zone heated by directly wind-driven turbulence.

6. COMPARISON WITH MODEL COMPUTATIONS

We now consider to what extent a one-dimensional mixed-layer model can describe the changes in heat content in the upper ocean. We have developed a simple one-dimensional mixed-layer model, the details of which can be found elsewhere (Prangsma & Kruseman 1982). A selection of the results of the model computations, obtained by starting from the temperature profile for survey 1 (figure 2) and using the same surface-forcing as in figure 4, is shown in figure 7, and the modelled heat contents are shown in figure 4 (triangles). From figure 7 we conclude that the computations model the averaged observations reasonably well. The quality of the model can be further assessed from the following statistics:

the sea surface temperature, obtained by averaging hourly observations for the two months of JASIN, is 12.6 ± 0.6 °C. The mean difference between the observed and computed hourly values is 0.0 ± 0.3 K

the mean observed heat content at 150 m (H(150 m)) is 6295 ± 73 MJ m^{-2}.

The mean difference for observed minus computed heat content is -35 ± 48 MJ m^{-2}. In our opinion this gives the conclusive argument for considering the averaged profiles obtained to be representative: a one-dimensional model, starting from an averaged profile and driven by

observed meteorological forcing, is able to describe the developments in the profile to well within the standard deviations of the averaging procedure, even in the presence of a residual eddy signal.

7. Summary

In this paper we have shown that it is possible to obtain average profiles of temperature and salinity that can be considered representative for an ocean area of about 100 km × 150 km covering several meoscale features. Total removal of the eddy signal from temperature profiles is found to be impossible owing to the eddy signal's varying with depth.

We have shown that on average the surface heat fluxes (50 W m^{-2}) balance the changes in the oceanic heat budget, advective terms being generally smaller by an order of magnitude (10 W m^{-2}) during most of the JASIN field experiment. Though measured currents were high, up to 26 cm s^{-1}, most of the flow was associated with the eddies and was contained within the 100 km × 150 km area, and did not lead to large transport of heat in or out of the area. On scales less than an eddy diameter (90 km), eddy advection (-400–300 W m^{-2}) dominated local changes in heat content.

A one-dimensional model is presented, capable of simulating the observed changes in the temperature profile.

We wish to thank the commander and crew members of Hr. Neth. Ms. *Tydeman* for their kind hospitality and excellent cooperation during the JASIN field phase; many of the data were prevented from being worthless by their continuing interest and assistance in solving numerous technical details.

References

Gill, A. E. 1975 Evidence of mid-ocean eddies in weather ship records. *Deep-Sea Res.* **22**, 647–652.

Kitaigorodskii, S. A. & Miropolskii, Y. Z. 1970 On the theory of the open-ocean active layer. *Izv. atmos. ocean. Phys.* **6**, 178–188.

Kruseman, P. & Prangsma, G. J. 1977 Some preliminary results from Hr. Neth. Ms. *Tydeman's* JASIN 1977 cruise. JASIN news, no. 5.

Kruseman, P. & Prangsma, G. J. 1979 Sea surface temperature and mixed layer depth during the JASIN 1978 experiment. KNMI Verslagen V-325. (Internal report.)

Kruseman, P. & Prangsma, G. J. 1982 Salinity variations in the upper ocean during JASIN. KNMI scientific report. (In preparation.)

Pollard, R. T. 1982*a* Mesoscale (50–100 km) circulations revealed by inverse and classical analysis of the JASIN hydrographic data. *J. phys. Oceanogr.* **12**, 1122–1136.

Pollard, R. T. 1982*b* Eddies and fronts in the JASIN area. JASIN news, no. 25.

Pollard, R. T., Rhines, P. B. & Thompson, R. O. R. Y. 1973 The deepening of the wind-mixed layer. *Geophys. Fluid Dyn.* **4**, 381–404.

Prangsma, G. J. & Kruseman, P. 1982 A simple, empirical heat conserving mixed layer model. (In preparation.)

Weller, R. A. 1982 The relation of near-inertial motions observed in the mixed layer during the JASIN (1978) experiment to the local wind stress and to the quasigeostrophic flow field. *J. phys. Oceanogr.* **12**, 1122–1136.

Discussion

G. Siedler (*Institut für Meereskunde, Düsternbrooker Weg* 20, *D*-2300 *Kiel, F.R.G.*). The 150 m level was selected as the lower boundary of the layer over which heat content changes were integrated. Would it not have been more appropriate to select a level between approximately 50 and 100 m where repeated CTD profiles lead to much less temperature variance than at 150 m?

G. J. Prangsma. The choice of the 150 m level as the lower boundary for integration of heat content changes is in a way very arbitrary indeed. The aims of the study one wants to pursue must, however, be borne in mind. If one chooses to model the changes on a short timescale (i.e. a few days at most) then the bottom of the seasonal thermocline (between 50 and 100 m) is the better candidate. If one is, however, interested in the seasonal timescale then a deeper level, where the radiative heat transfer is negligible even when integrated over a few months, is more appropriate. This last route has been followed in our study.

PHILOSOPHICAL TRANSACTIONS OF THE ROYAL SOCIETY A MATHEMATICAL, PHYSICAL & ENGINEERING SCIENCES